



1 **Size-resolved exposure risk of persistent free radicals (PFRs)**  
2 **in atmospheric aerosols and their potential sources**

3 Qingcai Chen,<sup>a</sup> Haoyao Sun,<sup>a</sup> Wenhui Song,<sup>b</sup> Fang Cao,<sup>b</sup> Chongguo Tian,<sup>c</sup> Yan-Lin  
4 Zhang<sup>b\*</sup>

5 <sup>a</sup> *School of Environmental Science and Engineering, Shaanxi University of Science and*  
6 *Technology, Xi'an 710021, China*

7 <sup>b</sup> *Yale–NUIST Center on Atmospheric Environment, International Joint Laboratory on Climate*  
8 *and Environment Change (ILCEC), Nanjing University of Information Science and Technology,*  
9 *Nanjing 210044, China*

10 <sup>c</sup> *Key Laboratory of Coastal Environmental Processes and Ecological Remediation, Yantai*  
11 *Institute of Coastal Zone Research, Chinese Academy of Sciences, Yantai, 264003, China*

12 \*Corresponding Author at: Ningliu Road 219, Nanjing 210044, China.

13 E-mail address: [dryanlinzhang@outlook.com](mailto:dryanlinzhang@outlook.com) or [zhangyanlin@nuist.edu.cn](mailto:zhangyanlin@nuist.edu.cn) (Yan-Lin Zhang).



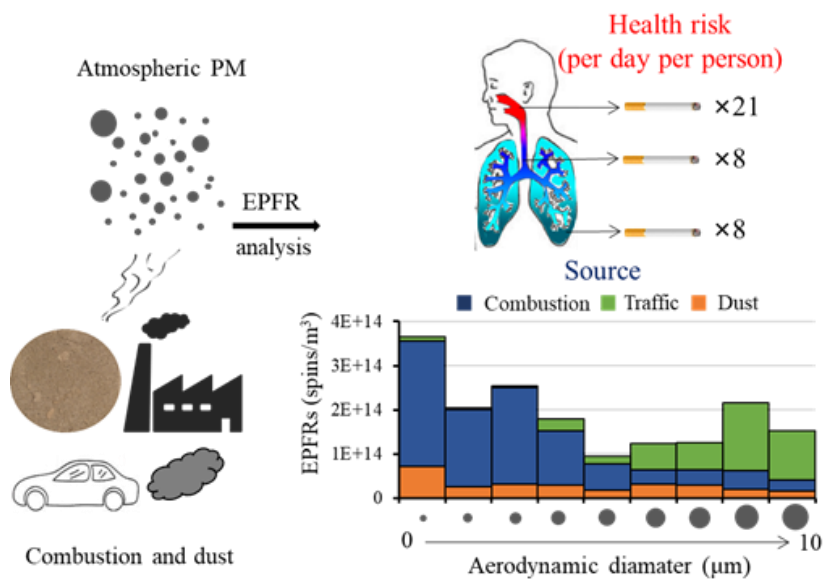
14 **Abstract:** Environmentally persistent free radicals (EPFRs) are a new type of  
15 substance with potential health risks. EPFRs are widely present in atmospheric  
16 particulates, but there is a limited understanding of the size-resolved health risks of  
17 these radicals. This study first reported the exposure risks and source of EPFRs in  
18 atmospheric particulate matter (PM) of different particle sizes ( $<10\ \mu\text{m}$ ) in Linfen, a  
19 typical coal-burning city in China. The type of EPFRs in fine particles ( $<2.1\ \mu\text{m}$ ) is  
20 different from that in coarse particles ( $2.1\text{-}10\ \mu\text{m}$ ) in both winter and summer.  
21 However, the EPFR concentration is higher in coarse particles than in fine particles in  
22 summer, and the opposite trend is found in winter. In both seasons, combustion  
23 sources are the main sources of EPFRs with coal combustion as the major contributor  
24 in winter, while biomass combustion is the major source in summer. Dust contributes  
25 part of the EPFRs and it is mainly present in coarse particles in winter and the  
26 opposite in summer. The upper respiratory tract was found to be the area with the  
27 highest risk of exposure to EPFRs of the studied aerosols, with an exposure equivalent  
28 to that of approximately 21 cigarettes per person per day. Alveolar exposure to EPFRs  
29 is equivalent to 8 cigarettes per person per day, with combustion sources contributing  
30 the most to EPFRs in the alveoli. This study helps us to better understand the potential  
31 health risks of atmospheric PM with different particle sizes.

32 **Key words:** EPFRs; particle size distribution; source; generation mechanism

33



34 TOC Art:



35



## 36 1. Introduction

37 Free radicals are atoms or groups containing unpaired electrons, such as hydroxyl  
38 radicals and superoxide radicals, and they usually have strong chemical reactivity and  
39 short lifetimes (Pryor et al., 1986; Finkelstein., 1982). Free radicals with long  
40 lifetimes (months or even years) in the environment are currently called  
41 environmentally persistent free radicals (EPFRs), which have received much attention  
42 in recent years as new environmentally hazardous substances (Vejerano et al., 2018;  
43 Gehling, 2013; Chen et al., 2019c). EPFRs can be used as an active intermediate to  
44 catalyze the production of reactive oxygen species (ROS) by oxygen molecules, thus  
45 endangering human health (D'Arienzo et al., 2017; Thevenot et al., 2013; Harmon et  
46 al., 2018; Blakley et al., 2001; Khachatryan et al., 2011). Studies have found that  
47 EPFRs are present in different environmental media, such as water and soil, and even  
48 in the atmosphere (Dellinger et al., 2001; Truong et al., 2010; Vejerano et al., 2012).

49 A number of studies have investigated the occurrences, sources and formation  
50 mechanisms of EPFRs in atmospheric particulates in different regions. For example,  
51 in the studies of Rostock in Germany, Taif in Saudi Arabia and Xuanwei in China, the  
52 average concentration of EPFRs in atmospheric particulate matter (PM) was reported  
53 to be in the range of  $\sim 10^{16}$  -  $10^{18}$  spins/g (Wang et al., 2018; Arangio et al., 2016;  
54 Shaltout et al., 2015). Atmospheric EPFRs are mainly carbon-centered radicals with  
55 adjacent oxygen atoms (Gehling et al., 2013). EPFRs of different lifetimes are present  
56 in atmospheric PM, with only a few hours for short-lifetime EPFRs and several years  
57 for long-lifetime EPFRs that show no signs of decay (Gehling et al., 2013; Chen et al.,  
58 2019c). Most studies indicate that sources of transportation and combustion may be  
59 the primary EPFR sources in atmospheric PM (Wang et al., 2018; Yang et al., 2017;  
60 Chen et al., 2019b). Chen et al. (2018b and 2019b) found that strong atmospheric  
61 photochemical effects in summer and dust particles may also be important sources of  
62 EPFRs. The process of electron transfer and stabilization between the surface of metal  
63 oxides (such as iron, copper, zinc and nickel) and substituted aromatic molecules



64 under high temperatures is considered to be the main mechanism for the formation of  
65 EPFRs in atmospheric particles (Truong., 2010; Vejerano et al., 2012a; Patterson et al.,  
66 2013; Vejerano., 2010; Vejerano et al., 2012b). However, the study by Chen et al.  
67 (2018a) suggests that EPFRs in atmospheric particulates are mainly derived from  
68 graphite oxide-like substances produced during combustion. In addition to primary  
69 sources such as combustion, secondary chemical processes in the atmosphere may  
70 also be an important source of EPFRs in atmospheric PM (Chen et al. 2019b and  
71 2019d; Tong et al., 2018).

72 Different particle sizes of atmospheric PM pose different health risks to humans,  
73 depending on the deposition efficiency of the particles and the chemical composition  
74 and concentrations of hazardous substances they contain (Strak et al., 2012;  
75 Valavanidis et al., 2008). Among various hazardous substances, EPFRs may also be  
76 involved in the toxicity of atmospheric particulates. Yang et al. (2017) studied the  
77 EPFRs that are extractable by dichloromethane in different particle sizes in Beijing in  
78 winter and found that the concentration of EPFRs was the highest in particles with  
79 sizes  $< 1 \mu\text{m}$ . Arangio et al. (2016) found that the concentration of EPFRs in 180 nm  
80 particles was the highest in the 56 nm - 1.8  $\mu\text{m}$  particle size range. Although several  
81 studies have examined the particle size distribution of EPFRs, systematic studies have  
82 not been conducted on the formation mechanism, source and exposure assessment of  
83 EPFRs in atmospheric particles with different particle sizes.

84 This study takes Linfen as an example. Linfen is one of the cities in China with  
85 the most serious air pollution and is a typical coal-burning city. The particle size  
86 distribution of EPFRs in atmospheric PM in this region was studied by EPR  
87 spectrometry. The effects of particle size and season on the source, formation  
88 mechanism, and health risk of EPFRs were revealed. In particular, the comprehensive  
89 health risks of EPFRs were evaluated, and it was found that the upper respiratory tract  
90 is the area with the highest risk of EPFRs exposure, which is equivalent to twenty-one  
91 cigarettes per person per day. This study is of great significance for understanding the  
92 source and formation mechanism of EPFRs in atmospheric particulates as well as for



93 health risk assessments.

## 94 **2. Experimental section**

### 95 *2.1 Sample collection*

96 The sampling site for this study is located in Hongdong (36°23', 111°40'E) in  
97 Shanxi, China. To collect atmospheric particles of different sizes (0-10  $\mu\text{m}$ ), this study  
98 used a Thermo-Anderson Mark II sampler to collect aerosol samples of 9 sizes. The  
99 samples were collected on a prebaked quartz filter (450 °C, 4.5 hours), and the  
100 sampling dates were as follows: in winter, January 26 to February 4, 2017,  $n = 10$ ; and  
101 in summer, July 31 to August 24, 2017,  $n = 12$ . The samples were placed in a -20 °C  
102 refrigerator prior to analysis.

### 103 *2.2 EPFR analysis*

104 Specific testing protocols have been described previously (Chen et al., 2018c. The  
105 sample filter was cut into thin strips and clamped with a quartz piece, and then the  
106 quartz piece with attached filter sample was placed in a resonant cavity and analyzed  
107 by an EPR spectrometer (MS5000, Freiberg, Germany). The detection parameters  
108 were magnetic field strength, 335 - 342 mT; detection time, 60 s; modulation  
109 amplitude, 0.20 mT; number of detections, 1; and microwave intensity, 8.0 mW.

### 110 *2.3 Carbon composition analysis*

111 The contents of organic carbon (OC) and elemental carbon (EC) in the filter  
112 samples were analyzed using a semicontinuous OC/EC analyzer (Model 4, Sunset Lab.  
113 Inc., Oregon, USA) with a NIOSH 5040 detection protocol (Lin et al., 2009).

114 The water-soluble organic carbon (WSOC) concentration was analyzed using an  
115 automatic TOC-LCPH analyzer (Shimadzu, Japan). The WSOC extraction was  
116 performed with ultrapure water under ultrasonication for 15 minutes, and all WSOC  
117 concentrations were blank corrected. The concentration of OC in the MSM  
118 (Methanol-soluble materials) was calculated as the difference between the OC and



119 WSOC (Water-soluble organic carbon) concentrations. This calculation assumes that  
120 all water-insoluble organic carbon (WISOC) in the aerosol can be extracted with  
121 MeOH, and the rationality of this assumption has been verified elsewhere (Mihara et  
122 al., 2011; Liu et al., 2013; Cheng et al., 2016; Chen et al., 2019a).

#### 123 *2.4 PAH analysis*

124 PAHs were detected using gas chromatography/mass spectrometry (GC/MS) on a  
125 GC7890B/MS5977A (Agilent Technologies, Clara, CA), as described in detail in a  
126 previously published study (Han et al., 2018).

#### 127 *2.5 Metal element analysis*

128 The concentration of metal elements in the samples was determined by a Thermo  
129 X2 series inductively coupled plasma mass spectrometer (ICP-MS, Thermo, USA).  
130 The metal elements analyzed in summer were Na, Mg, K, Ca, Ti, V, Cr, Mn, Fe, Co,  
131 Ni, Cu, Zn, As, Cd, Pb, and Al, and those in winter were Al, Zn, V, Cr, Mn, Co, Ni, Cu,  
132 As, Se, Sr, Cd, Ba, and Pb. The specific measurement method is based on the study of  
133 Qi et al (2016).

#### 134 *2.6. Data statistics method*

135 The source and formation mechanism of EPFRs in PM with different particle sizes  
136 were analyzed by nonnegative matrix factorization (NMF). The method is based on  
137 the study of Chen et al (2016 and 2019e). Briefly, NMF analysis of EPFR data, metal  
138 element contents, OC/EC contents and PAH contents was performed in MATLAB.  
139 The version of the NMF toolbox is 1.4 (<https://sites.google.com/site/nmftool/>). First, a  
140 gradient-based multiplication algorithm is used to find a solution from multiple  
141 random starting values, and then the first algorithm is used to find a solution to the  
142 final solution using a least squares effective set algorithm. To find a global solution,  
143 the model was run 100 times, each time with a different initial value. By comparing  
144 the 1-12 factor model (Figure S4) with the residual of the spectral load, the 6 factor  
145 (summer) and 10 factor (winter) NMF models were finally selected.



## 146 2.7. EPFR exposure evaluation

147 To assess the health risks of EPFRs, we divided the respiratory system into three  
148 parts based on the human breathing model: extrathoracic (ET) areas, including the  
149 anterior nasal cavity, posterior nasal cavity, oral cavity, and throat; tracheobronchial  
150 (TB) areas, including the trachea, bronchi, bronchioles, and terminal bronchi; and  
151 pulmonary (P) areas, including the alveolar ducts and alveoli. Then, the sedimentation  
152 rates of different particle sizes in different areas of the respiratory system were  
153 determined to calculate the exposure risk of EPFRs. Here, the human respiratory  
154 system particulate deposition model of Salma et al. (2002) was used, and the specific  
155 data can be found in Table S3 and S4.

156 In addition, we converted the daily inhaled concentration of EPFRs into the  
157 concentration of free radicals in cigarettes. The specific conversion method is as  
158 follows:

$$159 \quad N_{\text{cig}} = (C_{\text{EPFRs}} \cdot V) / (RC_{\text{cig}} \cdot C_{\text{tar}}) \quad (1)$$

160 where  $N_{\text{cig}}$  represents the number of cigarettes (/person/day),  $C_{\text{EPFRs}}$  ( $\text{spins}/\text{m}^3$ )  
161 represents the atmospheric concentration of EPFRs in PM, and  $V$  represents the  
162 amount of air inhaled by an adult per day ( $20 \text{ m}^3/\text{day}$ ) (Environmental Protection  
163 Agency, 1988).  $RC_{\text{cig}}$  ( $4.75 \times 10^{16} \text{ spins}/\text{g}$ ) (Baum et al., 2003; Blakley et al., 2001;  
164 Pryor et al., 1983; Valavanidis and Haralambous, 2001) indicates the concentration of  
165 free radicals in cigarette tar, and  $C_{\text{tar}}$  ( $0.013 \text{ g}/\text{cig}$ ) indicates the amount of tar per  
166 cigarette (Gehling et al., 2013).

## 167 3. Results and discussion

### 168 3.1 Concentrations and types of EPFRs

169 Figure 1a shows the concentration distribution of EPFRs with different particle  
170 sizes in different seasons. EPFRs were detected in the particles of each tested size (the  
171 EPR spectrum is shown in Figure S1), but their EPFR concentration levels were  
172 different. In summer, the concentration of EPFRs in fine particles (particle size  $< 2.1$





173  $\mu\text{m}$ ) is  $(3.2 - 8.1) \times 10^{13}$  spins/ $\text{m}^3$ , while the concentration of EPFRs in coarse  
174 particles (particle size  $> 2.1 \mu\text{m}$ ) is 1-2 orders of magnitude higher than that of fine  
175 particles, reaching values of  $(2.2 - 3.5) \times 10^{14}$  spins/ $\text{m}^3$ . Winter samples show  
176 completely different characteristics from summer samples. The concentration of  
177 EPFRs in fine particles (particle size  $< 2.1 \mu\text{m}$ ) is  $(1.8 - 3.6) \times 10^{14}$  spins/ $\text{m}^3$ , while the  
178 concentration of EPFRs in coarse particles (particle size  $> 2.1 \mu\text{m}$ ) is smaller than that  
179 of fine particles, with values of  $(1.0 - 2.1) \times 10^{14}$  spins/ $\text{m}^3$ . In addition, the  
180 concentration of EPFRs in particulates  $< 0.43 \mu\text{m}$  in winter is very high, but it is very  
181 low in summer. This particulate matter is related to combustion, which indicates that  
182 coal combustion in winter may provide an important contribution to EPFRs. The  
183 EPFR concentration in the fine PM of Linfen reported above is equivalent to that in  
184 the fine PM of Xi'an, but it is ten times smaller than that in the fine PM of Beijing  
185 (Yang et al., 2017; Chen et al., 2019b). Although the particle size distribution  
186 characteristics of EPFRs in winter and summer are different, their concentration levels  
187 are similar, which indicates that the EPFR concentration is not related to the PM  
188 concentration, but is determined by the source characteristics. The source  
189 characteristics will be discussed in detail in the factor analysis section.

190 Figure 1b shows the contribution of the EPFR concentration to the overall EPFR  
191 concentration in coarse and fine particles. The contribution of fine PM in summer is  
192 only 14.9%, while that of fine PM in winter is 58.5%. The differences in EPFR  
193 concentrations with particle size may be related to the source of EPFRs. For example,  
194 coarse particles are often associated with dust sources. In another study, we have  
195 shown that dust particles contain large amounts of EPFRs and that they can be  
196 transported over long distances (Chen et al., 2018b). EPFRs in fine particles may be  
197 mainly derived from the combustion process, such as traffic sources, which are  
198 considered to be an important source of EPFRs in atmospheric PM (Secrest et al.,  
199 2016; Chen et al., 2019b). Due to winter heating in the Linfen area, the amount of  
200 coal burning increases sharply in this season. In 2017, the nonclean heating  
201 (Coal-fired heating) rate of urban heating energy structures in Linfen was 40% (data



202 source: <http://www.linfen.gov.cn/>). With the burning of coal, large amounts of EPFRs  
203 are produced, and in the summer, EPFRs emitted by burning coal should be much less  
204 than those emitted in winter. This can explain to a certain extent that the contribution  
205 of fine particles to summer EPFRs is small, and the contribution of winter EPFRs is  
206 very large.

207 The  $g$ -factor is a parameter used to distinguish the type of EPFR (Shaltout et al.,  
208 2015; Arangio et al., 2016). The  $g$ -factor of carbon-centered persistent free radicals is  
209 generally less than 2.003, the  $g$  factor of oxygen-centered persistent radicals is  
210 generally greater than 2.004, and the  $g$  factor of carbon-centered radicals with  
211 adjacent oxygen atoms is between 2.003 and 2.004 (Cruz et al., 2012). Figure 2a  
212 shows the  $g$ -factor distribution characteristics of EPFRs in different particle sizes in  
213 summer and winter. The  $g$ -factor of fine particles and coarse particles also shows  
214 different characteristics. The  $g$ -factor of EPFRs in fine particles (particle size  $< 2.1$   
215  $\mu\text{m}$ ) ranges from 2.0034 to 2.0037, which may be from carbon-centered radicals with  
216 adjacent oxygen atoms. However, the  $g$ -factor of EPFRs in coarse particles (particle  
217 size  $> 2.1 \mu\text{m}$ ) is significantly less than that of fine particles. The  $g$ -factor ranges from  
218 2.0031 to 2.0033, indicating that EPFRs in coarse particles are more carbon-centered  
219 than those in fine particles and are free of heteroatoms. Although the particle size  
220 characteristics of the  $g$ -factor of the EPFRs in summer and winter are the same, the  
221 variation in the  $g$ -factor with concentration is different. As shown in Figure 2b, the  
222  $g$ -factor of summer PM showed a significant decreasing trend with increasing  
223 concentration, while the  $g$ -factor of winter PM showed a significant increasing trend  
224 with increasing EPFR concentration. Oyana et al. (2017) studied EPFRs in the surface  
225 dust of leaves in the Memphis region of the United States and found that the  
226 concentration of EPFRs was positively correlated with the  $g$ -factor, and they believed  
227 that this was related to the source of EPFRs. This phenomenon indicates that the  
228 sources and toxicity of EPFRs in winter and summer are different. Figure 1 shows  
229 that the summer EPFRs are mainly derived from coarse particles, while the  $g$ -factor of  
230 EPFRs in coarse particles is smaller than that in fine particles, so the  $g$ -factor of



231 EPFRs in summer decreases with an increase in EPFR concentration. In winter, fine  
232 particles contribute more to EPFRs, so the *g*-factor of EPFRs in winter increases with  
233 the concentration of EPFRs.

### 234 *3.2 Factor Analysis of EPFRs*

235 To explore the possible sources and formation mechanism of EPFRs in atmospheric  
236 particles with different particle sizes, the NMF model was used to statistically analyze  
237 EPFRs, carbon components, PAHs and metal elements in samples. The factors  
238 obtained by the NMF model should reflect the different sources mechanisms of  
239 EPFRs. As shown in Figure 3a1 and b1, the three main contributing factors to EPFRs  
240 in summer and winter are shown (see Figure S5, S6 for spectra of other factors),  
241 which explain 94.5% and 83.8% of the EPFR concentrations in summer and winter,  
242 respectively.

243 As shown in Figure 3a, the typical spectral characteristic of summer factor 1 is that  
244 it contains a small fraction of EC components and a large amount of OC components,  
245 which indicates that combustion may be the source associated with this factor. This  
246 factor has the highest loading of OC, especially WISOC; this fraction mainly contains  
247 macromolecular organic substances, which are considered to contribute to the main  
248 atmospheric particulate EPFRs and to be graphite oxide-like substances (Chen et al.,  
249 2017; Chen et al., 2018a). The result shows that factor 1 has the highest contribution  
250 of all the factors to EPFRs in PM (69.6%), and they are mainly distributed in particles  
251 with sizes  $> 2.1 \mu\text{m}$ . Factor 2 is typically characterized by a high contribution from  
252 EC and a small fraction of OC and metal elements, which is a typical source of  
253 incomplete combustion. Factor 2 is different from factor 1; factor 2 is more likely the  
254 combustion of fossil fuels, while factor 1 may be biomass combustion source. The  
255 generation mechanism is similar to a hybrid mechanism, which includes the graphite  
256 oxide-like substances produced by incomplete combustion and the EPFRs formed by  
257 some metal oxides. The relative contribution of these EPFRs is 13.5% and is mainly  
258 distributed in particles with a size  $< 0.43 \mu\text{m}$ . The typical characteristic of factor 3 is  
259 that the contribution of metal elements is relatively high, while the contributions of



260 EC and OC are very low. Metal elements such as Al, Ti, Mn, and Co are typical crust  
261 elements, so this factor may represent dust sources (Pan et al., 2013; Srivastava et al.,  
262 2007; Trapp et al., 2010). The generation mechanism may be mainly due to the  
263 participation of metal oxides in the generation of EPFRs. Compared with the other  
264 factors, this factor also has a partial load on PAHs, indicating that PAHs may be  
265 involved in the formation of metal oxide-related EPFRs. These EPFRs have a  
266 relatively low contribution to total EPFRs (approximately 12.4%) and are mainly  
267 distributed in particles with a size of 0.43 - 2.1  $\mu\text{m}$ . The EPFR contribution of other  
268 factors is 4.4%; they are likely derived from the electroplating metallurgy industry  
269 (detailed in S1).

270 The results of the factor analysis in winter are different from those in summer. As  
271 shown in Figure 3b, the typical spectral characteristic of factor 1 is that it contains a  
272 large amount of OC components and As and Se. As and Se are trace elements of coal  
273 combustion, as shown in many studies (Pan et al., 2013; Tian et al., 2010), so coal  
274 combustion may be the source represented by this factor. From the generation  
275 mechanism viewpoint, the factor does not contain EC, but the content of OC is very  
276 high. In the particles with a particle size of less than 3.3, which is mainly present in  
277 factor 1, the concentration of OC is 16 times that of EC. So it may be mainly a  
278 graphite oxide-like substance formed by the agglomeration of gaseous volatile organic  
279 compounds (VOCs) generated during combustion. These EPFRs are mainly  
280 distributed in particles with a size of 0.43 - 3.3  $\mu\text{m}$ , and their contribution to EPFRs in  
281 PM is up to 44.6%. Factor 2 contributes 25.7% to EPFRs. The typical spectral  
282 characteristics are due to a large amount of V and some Al, EC and OC. OC and EC  
283 are also typical combustion products. V is rich in fossil fuels, especially fuel oil  
284 (Karnaev et al., 2011). Therefore, traffic is the source represented by this factor. The  
285 factor contains crust elements such as Al and Mn, so it is speculated that this factor  
286 may also include traffic-related dust. The particle size distribution shows that such  
287 EPFRs are mainly present in large particles with a size of 3.3 - 10  $\mu\text{m}$ . The typical  
288 spectral characteristics of factor 3 are similar to those of factor 1, and both contain



289 relatively large amounts of As and Se, with the exception that factor 3 contains a large  
290 amount of EC, indicating that it is also mainly derived from incomplete combustion  
291 sources. The generation mechanism of factor 3 should be different from factor 1,  
292 which may include both the graphite oxide-like material generated by fuel coking and  
293 the EPFRs generated by the metal oxide. These EPFRs are mainly distributed in  
294 particles with a size of  $<0.43 \mu\text{m}$ , and their total contribution to EPFRs in PM is  
295 13.4%. In addition, the other factors contribute 16.3% to EPFRs, and these factors are  
296 mainly atmospheric dust (11.4%) and electroplating or metallurgy (4.9%) (see text  
297 S1). The results of this study factor analysis were similar to the results of the study by  
298 Wang et al. (2019) on EPFRs in Xi'an. They found that coal, traffic and dust were the  
299 main sources of EPFRs and accounted for 76.2% of the total source.

300 Based on the above analysis, it can be found that combustion sources are the main  
301 sources of EPFRs, and EPFRs from these sources are mainly graphite oxide-like  
302 substances generated by the polymerization of organic matter or fuel coking. Studies  
303 have shown that graphene oxide can cause cell damage by generating ROS (Seabra et  
304 al., 2014). The surface of these compounds contains not only carbon atoms but also  
305 some heteroatoms, which leads to disorder and the presence of defects in the  
306 carbon-based structure (Lyu et al., 2018; Chen et al., 2017a; Mukome et al., 2013;  
307 Keiluweit et al., 2010). The dust source is also a source of important EPFRs identified  
308 in this study (with a contribution of approximately 10%). It was shown in the above  
309 analysis that the concentration of EPFRs in coarse particles has a significant  
310 correlation with the concentration of metallic elements, particularly crustal elements.  
311 Some crustal elements, such as Al, and Fe, not only have their own paramagnetism  
312 (Li et al., 2017; Yu et al., 2013; Nikitenko et al., 1992), but also interact with aromatic  
313 compounds attached to the surface of the particles to produce a stable single-electron  
314 structure.

### 315 3.3 Health risk of EPFRs

316 To evaluate the health risks of EPFRs in PM with different particle sizes, we



317 evaluated the comprehensive exposure of EPFRs based on the deposition efficiency of  
318 PM with different particle sizes in different parts of the human body. The results are  
319 shown in Figure 4a. The ET region is the region with the highest EPFR exposure,  
320 while the TB and P regions have relatively close EPFRs. This result shows that  
321 atmospheric EPFRs are the most harmful to the health of the human upper respiratory  
322 tract. Comparing the EPFR exposure in different seasons indicates that the exposure  
323 risk in the ET area in summer is significantly higher than that in winter. This  
324 difference occurs because the concentration of EPFRs in coarse particles is much  
325 higher than that of fine particles in summer and the deposition efficiency of large  
326 particles in the ET area is generally higher. Fine particles are more efficiently  
327 deposited in the P region, leading to a higher risk of EPFR exposure in the P region in  
328 winter.

329 EPFRs were first found in cigarette tar and are considered one of the health risk  
330 factors in cigarette smoke (Lyons et al., 1960); thus, in this study, the exposure risks  
331 of EPFRs in particles deposited in the human body were converted to the equivalent  
332 number of cigarettes inhaled per adult per day. As shown in Figure 4b, the ET area is  
333 the most contaminated area, with an average equivalence of twenty-one cigarettes  
334 (twenty-five in summer and sixteen in winter). The average values for the TB area  
335 (nine in summer and seven in winter) and P area (seven in summer and ten in winter)  
336 are eight. The results indicate that EPFRs pose significant health risks to human lungs  
337 in both winter and summer. Other similar studies, such as a study of the average  
338 amount of EPFRs in  $PM_{2.5}$  inhaled per person per day in Xi'an in 2017, found values  
339 equivalent to approximately 5 cigarettes (Chen et al., 2018a). Gehring et al. (2013)  
340 found that EPFR exposure in  $PM_{2.5}$  is equivalent to approximately 0.3 cigarettes per  
341 person per day in St. Joaquin County, the location with the worst air pollution in the  
342 United States. The average exposure risk of EPFRs in fine particles in the Linfen area  
343 (approximately 13 cigarettes) was higher than those in these two studies. However,  
344 these previous studies only studied the exposure risk of EPFRs in fine particles. The  
345 results of this study indicate that the health risks of EPFRs are significantly increased



346 when the particle size distribution of EPFRs is taken into account. Therefore, it is  
347 important to study the source characteristics and generation mechanism of EPFRs  
348 with different particle sizes, which will be discussed in detail in the following  
349 sections.

350 This study calculated the proportion of EPFRs with different particle sizes in  
351 different parts of the respiratory system based on the deposition efficiency of particles  
352 with different particle sizes. As shown in Figure 4c, in the ET region and the TB  
353 region, coarse particles are the dominant component in summer and winter. In  
354 particular, in summer, the proportion of EPFRs in coarse particles in these two regions  
355 exceeds 95%. In the P region, there are significant differences between summer and  
356 winter. The P region in summer is still dominated by coarse particles, but its  
357 proportion is significantly lower than those in the ET and TB regions. In the P region  
358 in winter, fine particles are the dominant component (approximately 70%). These  
359 distribution characteristics indicate different sources of EPFRs in different regions. As  
360 shown in Figure 4d, in summer, combustion sources are the main source of EPFRs in  
361 the respiratory system. In winter, combustion and transportation sources contribute  
362 equally in the EP and ET regions, while in the alveoli, combustion sources are the  
363 main contributor. The ET region is the area with the highest risk of exposure to  
364 EPFRs (21 cigarettes). The generation mechanism of these EPFRs is mainly  
365 attributable to graphene oxide-like substances. Studies have shown that graphene  
366 oxide is cytotoxic (Harmon et al., 2018). In the alveoli, the contribution of  
367 combustion sources is significantly increased (especially in winter). These EPFRs are  
368 mainly generated by the action of metal oxides and organic substances. Studies have  
369 shown that such EPFRs can generate ROS in the lung fluid environment (Khachatryan  
370 et al., 2011). Therefore, the health risks of EPFRs from different sources and  
371 mechanisms should be evaluated in the future in order to better assess the harm  
372 caused by EPFRs to the body.

#### 373 4. Conclusions and environmental implications



374 This study systematically reported the particle size distribution of EPFRs in  
375 atmospheric PM in Linfen, which is one of the most polluted cities in China and is  
376 located in a typical coal-burning area. In addition, this study evaluated the  
377 comprehensive health risks of EPFRs, and reported possible sources and formation  
378 mechanisms of atmospheric EPFRs with respect to different particle sizes. The  
379 following main conclusions were obtained.

380 (1) This study found that EPFRs are widely present in atmospheric particles of  
381 different particle sizes and exhibit significant particle size distribution characteristics.  
382 EPFR concentrations are higher in coarse particles than in fine particles in summer  
383 and vice versa in winter. Differences were also found in the g-factors of EPFRs in  
384 coarse particles and fine particles, indicating that the types of EPFRs of different  
385 particle sizes were also different. The results of this study demonstrate that the  
386 concentrations and types of EPFRs are dependent on particle size and season. This  
387 result indicates that the potential toxicity caused by EPFRs may also vary with  
388 particle size and season.

389 (2) This study reported the possible source and formation mechanisms of  
390 atmospheric EPFRs in different particle sizes. The results show that combustion is the  
391 most important source of EPFRs (>70%) in both winter and summer PM samples in  
392 Linfen. Atmospheric dust also contributes to EPFRs (~10%), and they are mainly  
393 found in fine particles in summer and coarse particles in winter. The graphite  
394 oxide-like mechanism has the highest contribution (~70%) and is mainly distributed  
395 in particles with a size of  $> 0.43 \mu\text{m}$ , while EPFRs in which metal oxides participate  
396 are mainly distributed in particles with a size of  $< 0.43 \mu\text{m}$ . These findings deepen our  
397 understanding of the pollution characteristics of atmospheric EPFRs and are useful for  
398 controlling EPFR generation in heavily polluted areas.

399 (3) This study assessed the exposure risk of EPFRs in different areas of the  
400 respiratory system. The results show that the upper respiratory tract is the area with  
401 the highest EPFR exposure (the value in summer is higher than that in winter), with a  
402 value equivalent to 21 cigarettes per person per day. EPFRs are equally exposed to the





403 trachea and alveoli, and the risk of exposure is equivalent to that of 8 cigarettes per  
404 person per day. Coarse particles are the main source of EPFRs in the upper respiratory  
405 tract, while fine particles are mainly involved in the alveoli. In summer, combustion  
406 sources are the main source of EPFRs in various parts of the respiratory system. In  
407 winter, traffic and other combustion sources are the main source of EPFRs in the  
408 upper respiratory tract, and combustion sources mainly contribute to the EPFRs in the  
409 alveoli.

410 Through this study, we have shown that there are significant differences in the  
411 concentrations and types of EPFRs in particles of different sizes and these differences  
412 are due to the influence of the source and generation mechanism. In the future,  
413 assessments of the particle size distribution and the seasonality of EPFRs in  
414 atmospheric PM should be considered. Health risks are another focus of this study.  
415 We found that the upper respiratory tract is the key exposure area of EPFRs, and the  
416 traffic source is the main source of EPFRs in this area. This finding is significant for a  
417 systematic assessment of the health risks of EPFRs. In view of the complexity and  
418 diversity of the formation mechanisms of EPFRs in actual atmospheric particulates,  
419 the relative contributions of EPFRs generated by different mechanisms and their  
420 associated health risks should be more comprehensively studied in the future.

#### 421 **Acknowledgments**

422 This work was supported by the National Natural Science Foundation of China  
423 (grant numbers: 41877354, 41761144056 and 41703102), the Provincial Natural  
424 Science Foundation of Jiangsu grant no. BK20180040), the Natural Science  
425 Foundation of Shaanxi Province, China (2018JM4011) and the fund of Jiangsu  
426 Innovation & Entrepreneurship Team.

#### 427 **Appendix A. Supplementary data**

428 Appendix A contains additional details, including the EPR spectra of samples of  
429 different particle sizes, correlations between EPFRs and carbon in particles of  
430 different particle sizes, the results and errors of factor analysis, correlation analysis of



431 EPFRs with metallic elements, and EPFR exposure in different areas of the human  
432 respiratory tract.

433 **Code/Data availability:** All data that support the findings of this study are  
434 available in this article and its Supplement or from the corresponding author on  
435 request.

436 **Author contribution:** Qingcai Chen: Research design, Methodology, Writing -  
437 Original Draft, Writing - Review & Editing, Project administration, Funding  
438 acquisition; Haoyao Sun: Investigation, Sample analysis, Writing - Original Draft,  
439 Writing - Review & Editing, Methodology, Formal analysis; Wenhui Song:  
440 Investigation, Sample collection, Chemical analysis; Fang Cao: Investigation, Sample  
441 collection; Chongguo Tian: Investigation, Chemical analysis; Yan-Lin Zhang:  
442 Conceptualization, Writing - Review & Editing, Formal analysis, Validation, Funding  
443 acquisition.

444 **Competing interests:** The authors declare that they have no conflict of interest.

## 445 **References**

- 446 Arangio, A. M., Tong, H., Socorro, J., Pöschl, U., Shiraiwa, M., 2016. Quantification of  
447 environmentally persistent free radicals and reactive oxygen species in atmospheric aerosol  
448 particles. *Atmos. Chem. Phys.* 16 (20), 13105–13119.
- 449 Blakley, R. L., Henry, D. D., Smith, C. J., 2001. Lack of correlation between cigarette mainstream  
450 smoke particulate phase radicals and hydroquinone yield. *Food. Chem. Toxicol.* 39 (4),  
451 401–406.
- 452 Baum, S.L., Anderson, I.G.M., Baker, R.R., Murphy, D.M., Rowlands, C.C., 2003. Electron spin  
453 resonance and spin trap investigation of free radicals in cigarette smoke: development of a  
454 quantification procedure. *Anal. Chim. Acta* 481, 1–13.
- 455 Cruz, A.L.N.D., Cook, R.L., Lomnicki, S.M., Dellinger, B., 2012. Effect of low temperature  
456 thermal treatment on soils contaminated with pentachlorophenol and environmentally  
457 persistent free radicals. *Environ. Sci. Technol.* 46, 5971–5978.
- 458 Chen, N., Huang, Y., Hou, X., Ai, Z., Zhang, L., 2017. Photochemistry of hydrochar: Reactive  
459 oxygen species generation and sulfadimidine degradation. *Environ. Sci. Technol.* 51 (19),  
460 11278–11287.
- 461 Chen, Q., Mu, Z., Song, W., Wang, Y., Yang, Z., Zhang, L., Zhang, Y., 2019a. Size-resolved  
462 characterization of the chromophores in atmospheric particulate matter in Linfen, China. *J.*  
463 *Geophys. Res-Atmos.* 124, DIO: 10.1029/2019JD031149.



- 464 Chen, Q., Ikemori, F., Nakamura Y., Vodicka, P., Kawamura, K., Mochida, M., 2017. Structural  
465 and light-absorption characteristics of complex water-insoluble organic mixtures in urban  
466 submicron aerosols. *Environ. Sci. Technol.* 51(15), 8293–8303.
- 467 Chen, Q., Miyazaki, Y., Kawamura, K., Matsumoto, K., Coburn, S., Volkamer, R., Iwamoto, Y.,  
468 Kagami, S., Deng, Y., Ogawa, S., 2016. Characterization of chromophoric water-soluble  
469 organic matter in urban, forest, and marine aerosols by HR-ToF-AMS analysis and  
470 excitation–emission matrix spectroscopy. *Environ. Sci. Technol.* 50 (19), 10351–10360.
- 471 Chen, Q., Sun, H., Mu, Z., Wang, Y., Li, Y., Zhang, L., Wang, M., Zhang, Z., 2019b.  
472 Characteristics of environmentally persistent free radicals in PM2.5: Concentrations, species  
473 and sources in Xi'an, Northwestern China. *Environ. Pollut.* 247, 18–26.
- 474 Chen, Q., Sun, H., Wang, J., Shan, M., Xue, J., Yang, X., Deng, M., Wang, Y., Zhang, L., 2019c.  
475 Long-life type — The dominant fraction of EPFRs in combustion sources and ambient fine  
476 particles in Xi'an. *Atmos. Environ.* 219, 117059.
- 477 Chen, Q., Sun, H., Wang, M., Mu, Z., Wang, Y., Li, Y., Wang, Y., Zhang, L., Zhang, Z., 2018a.  
478 Dominant fraction of EPFRs from Nonsolvent-Extractable organic matter in fine particulates  
479 over Xi'an, China. *Environ. Sci. Technol.* 52 (17), 9646–9655.
- 480 Chen, Q., Sun, H., Wang, M., Wang, Y., Zhang, L., Han, Y., 2019d. Environmentally persistent  
481 free radical (EPFR) formation by visible-light illumination of the organic matter in  
482 atmospheric particles. *Environ. Sci. Technol.* 53 (17), 10053–10061.
- 483 Chen, Q., Wang, M., Sun, H., Wang, X., Wang, Y., Li, Y., Zhang, L., Mu, Z., 2018b. Enhanced  
484 health risks from exposure to environmentally persistent free radicals and the oxidative stress  
485 of PM2.5 from asian dust storms in erenhot, Zhangbei and Jinan, China. *Environ. Int.* 123,  
486 260–268.
- 487 Chen, Q., Wang, M., Wang, Y., Zhang, L., Li, Y., Han, Y., 2019e. Oxidative potential of  
488 water-soluble matter associated with chromophoric substances in PM2.5 over Xi'an, China.  
489 *Environ. Sci. Technol.* 53 (17), 10053–10061.
- 490 Chen, Q., Wang, M., Wang, Y., Zhang, L., Xue, J., Sun, H., Mu, Z., 2018c. Rapid determination of  
491 environmentally persistent free radicals (EPFRs) in atmospheric particles with a quartz  
492 sheet-based approach using electron paramagnetic resonance (EPR) spectroscopy. *Atmos.*  
493 *Environ.* 184, 140–145.
- 494 Cheng, Y., He, K. B., Du, Z. Y., Engling, G., Liu, J. M., Ma, Y. L., Zheng, M., Weber, R. J., 2016.  
495 The characteristics of brown carbon aerosol during winter in Beijing. *Atmos. Environ.* 127,  
496 355–364.
- 497 Cormier, S. A., Lomnicki, S., Backes, W., Dellignier, B., 2006. Origin and health impacts of  
498 emissions of toxic by-products and fine particles from combustion and thermal treatment of  
499 hazardous wastes and materials. *Environ. Health Perspect.* 114 (6), 810–817.
- 500 D'Arienzo, M., Gamba, L., Morazzoni, F., Cosention, U., Creco, C., Lasagni, M., Pitea, D., Moro,  
501 G., Cepek, C., Butera, V., Sicilia, E., Russo, N., Muñoz-García, A., Pavone, M., 2017.  
502 Experimental and theoretical investigation on the catalytic generation of environmentally  
503 persistent free radicals from benzene. *J. Phys. Chem. A.* 121 (17), 9381–9393.
- 504 Dellinger, B., Lomnicki, S., Khachatryan, L., Maskos, Z., Hall, R. W., Adoukpe, J., McFerrin, C.,  
505 Truong, H., 2007. Formation and stabilization of persistent free radicals. *Proc. Combust. Inst.*  
506 31 (1), 521–528.



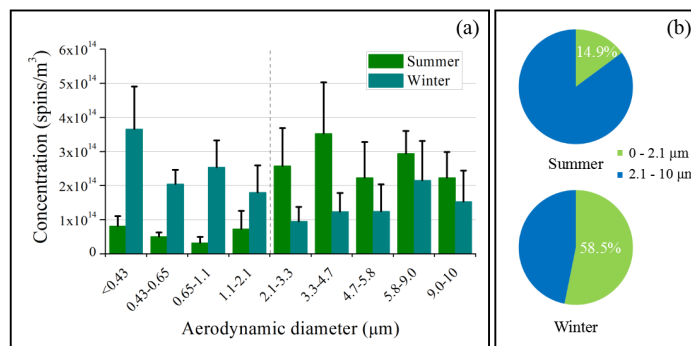
- 507 Dellinger, B., Pryor, W. A., Cueto, R., Squadrito, G. L., Hegde, V., Deutsch, W. A., 2001. Role of  
508 free radicals in the toxicity of airborne fine particulate matter. *Chem. Res. Toxicol.* 14 (10),  
509 1371–1377.
- 510 Environmental Protection Agency, 1988. Recommendations for and Documentation of Biological  
511 Values for Use in Risk Assessment. PB-179874. EPA 600/6-87/008. US Environmental  
512 Protection Agency, Cincinnati, OH.
- 513 Finkelstein, E., Rosen, G. M., Rauckman, E. J., 1982. Production of hydroxyl radical by  
514 decomposition of superoxide spin-trapped adducts. *Mol. Pharmacol.* 21 (2), 262–265.
- 515 Gehling, W., Dellinger, B., 2013. Environmentally persistent free radicals and their lifetimes in  
516 PM<sub>2.5</sub>. *Environ. Sci. Technol.* 47 (15), 8172–8178.
- 517 Han, Y., Chen, Y. J., Saud, A., Feng, Y. L., Zhang, F., Song, W. H., Cao, F., Zhang, Y., Yang, X., Li,  
518 J., Zhang, G., 2018. High time- and size-resolved measurements of PM and chemical  
519 composition from coal combustion: Implications for the EC formation process. *Environ. Sci.*  
520 *Technol.* 52 (11), 6676–6685.
- 521 Harmon, A. C., Hebert, V. Y., Cormier, S. A., Subramanian, B., Reed, J. R., Backes, W. L., Dugas,  
522 T. R., 2018. Particulate matter containing environmentally persistent free radicals induces  
523 AhR-dependent cytokine and reactive oxygen species production in human bronchial  
524 epithelial cells. *Plos. One.* 13 (10), e0205412.
- 525 Karnae, S., John, K., 2011. Source apportionment of fine particulate matter measured in an  
526 industrialized coastal urban area of South Texas. *Atmos. Environ.* 45 (23), 3769–3776.
- 527 Keiluweit, M., Nico, P. S., Johnson, M. G., Kleber, M., 2010. Dynamic molecular structure of  
528 plant biomass-derived black carbon (biochar). *Environ. Sci. Technol.* 44 (4), 1247–1253.
- 529 Khachatryan, L., Dellinger, B., 2011. Environmentally persistent free radicals (EPFRs)-2. Are free  
530 hydroxyl radicals generated in aqueous solutions?. *Environ. Sci. Technol.* 45 (21),  
531 9232–9239.
- 532 Li, G. L., Wu, S. Y., Kuang, M. Q., Hu, X. F., Xu, Y. Q., 2017. Studies on the g-factors of the  
533 copper(II)-oxygen compounds. *J. Struct. Chem.* 58 (4), 700–705.
- 534 Lin, P., Hu, M., Deng, Z., Slanina, J., Han, S., Kondo, Y., Takegawa, N., Miyazaki, Y., Zhao, Y.,  
535 Sugimoto, N., 2009. Seasonal and diurnal variations of organic carbon in PM<sub>2.5</sub> in Beijing  
536 and the estimation of secondary organic carbon. *J. Geophys. Res.-Atmos.* 114, 1–41.
- 537 Liu, J., Bergin, M., Guo, H., King, L., Kotra, N., Edgerton, E., Weber, R. J., 2013. Size-resolved  
538 measurements of brown carbon in water and methanol extracts and estimates of their  
539 contribution to ambient fine-particle light absorption. *Atmos. Chem. Phys.* 13, 12389–12404.
- 540 Lomnicki, S., Truong, H., Vejerano, E., Dellinger, B., 2008. Copper oxide-based model of  
541 persistent free radical formation on combustion-derived particulate matter. *Environ. Sci.*  
542 *Technol.* 42 (13), 4982–4988.
- 543 Lyu, L., Yu, G., Zhang, L., Hu, C., Sun, Y., 2018. 4-Phenoxyphenol-functionalized reduced  
544 graphene oxide nanosheets: A metal-free fenton-like catalyst for pollutant destruction.  
545 *Environ. Sci. Technol.* 52 (2), 747–756.
- 546 Lyons, M.J., Spence, J.B., 1960. Environmental free radicals. *Br. J. Canc.* 14, 703–708
- 547 Mihara, T., Michihiro, M., 2011. Characterization of solvent-extractable organics in urban aerosols  
548 based on mass spectrum analysis and hygroscopic growth measurement. *Environ. Sci.*  
549 *Technol.* 45 (21), 9168–9174.



- 550 Mukome, F. N. D., Zhang, X., Silva, L. C. R., Six, J., Parikh, S. J., 2013. Use of Chemical and  
551 physical characteristics to investigate trends in biochar feedstocks. *J. Agric. Food Chem.* 61  
552 (9), 2196–2204.
- 553 Nikitenko, V. A., 1992. Luminescence and EPR of zinc oxide (review). *J. Appl. Spectrosc.* 57  
554 (5–6), 783–798.
- 555 Oyana, T. J., Lomnicki, S. M., Guo, C., Cormier, S. A., 2017. A scalable field study protocol and  
556 rationale for passive ambient air sampling: a spatial phytosampling for leaf data collection.  
557 *Environ. Sci. Technol.* 51 (18), 10663–10673.
- 558 Pan, Y., Wang, Y., Sun, Y., Tian, S., Cheng, M., 2013. Size-resolved aerosol trace elements at a  
559 rural mountainous site in Northern China: importance of regional transport. *Sci. total Environ.*  
560 461–462, 761–771.
- 561 Patterson, M. C., Keilbart, N. D., Kiruri, L. W., Thibodeaux, C. A., Lomnicki, S., Kurtz, R. L.,  
562 Poliakoff, E. D., Dellinger, B., Sprunger, P. T., 2013. EPFR formation from phenol adsorption  
563 on Al<sub>2</sub>O<sub>3</sub> and TiO<sub>2</sub>: EPR and EELS studies. *Chem. Phys.* 422, 277–282.
- 564 Pryor, W.A., Prier, D.G., Church, D.F., 1983. Electron-spin resonance study of mainstream and  
565 sidestream cigarette smoke: nature of the free radicals in gas-phase smoke and in cigarette tar.  
566 *Environ. Health Perspect.* 47, 345–355.
- 567 Pryor, W. A., 1986. Oxy-Radicals and Related Species: Their Formation, Lifetimes, and Reactions.  
568 *Annu. Rev. Physiol.* 48, 657–667.
- 569 Qi, L., Zhang, Y., Ma, Y., Chen, M., Ge, X., Ma, Y., Zheng, J., Wang, Z., Li, S., 2016. Source  
570 identification of trace elements in the atmosphere during the second Asian Youth Games in  
571 Nanjing, China: Influence of control measures on air quality. *Atmos. Pollut. Res.* 7, 547–556.
- 572 Shaltout, A. A., Boman, J., Shehadeh, Z. F., Al-Malawi, D. A. R., Hemeda, O. M., Morsy, M. M.,  
573 2015. Spectroscopic investigation of PM<sub>2.5</sub>, collected at industrial, residential and traffic  
574 sites in taif. Saudi Arabia. *J. Aerosol. Sci.* 79, 97–108.
- 575 Srivastava, A., Jain, V. K., 2007. Size distribution and source identification of total suspended  
576 particulate matter and associated heavy metals in the urban atmosphere of Delhi.  
577 *Chemosphere.* 68(3), 579–589.
- 578 Strak, M., Janssen, N. A. H., Godri, K. J., Gosens, I., Mudway, I. S., Cassee, F. R., Lebret, E.,  
579 Kelly F. J., Harrison, R. M., Brunekreef, B., Steenhof, M., Hoek, G., 2012. Respiratory health  
580 effects of airborne particulate matter: The role of particle size, composition, and oxidative  
581 potential—the RAPTES project. *Environ. Health Persp.* 120 (8), 1183–1189.
- 582 Salma, I., Balásházy, I., Winkler-Heil, R., Hofmann, W., Zárny, G. 2002. Effect of particle mass  
583 size distribution on the deposition of aerosols in the human respiratory tract. *J. Aerosol. Sci.*  
584 33(1), 119–132.
- 585 Seabra A.B., Paula A.J., Lima R. D., Alves. O.L., Durán. N. 2014. Nanotoxicity of graphene and  
586 graphene oxide. *Chem. Res. Toxicol.* 27 (2), 159–168.
- 587 Thevenot, P. T., Saravia, J., Jin, N., Giaimo, J. D., Chustz, R. E., Mahne, S., Kelley, M. A., Hebert,  
588 V. Y., Dellinger, B., Dugas, T. R., Demayo, F. G., Cormier, S. A., 2013. Radical-containing  
589 ultrafine particulate matter initiates epithelial-to-mesenchymal transitions in airway epithelial  
590 cells. *Am. J. Respir. Cell. Mol. Biol.* 48 (2), 188–197.
- 591 Tian, H., Wang, Y., Xue, Z., Cheng, K., Qu, Y., Chai, F., Hao, J., 2010. Trend and characteristics of  
592 atmospheric emissions of Hg, As, and Se from coal combustion in China, 1980–2007. *Atmos.*  
593 *Chem. Phys.* 10 (23), 11905–11919.

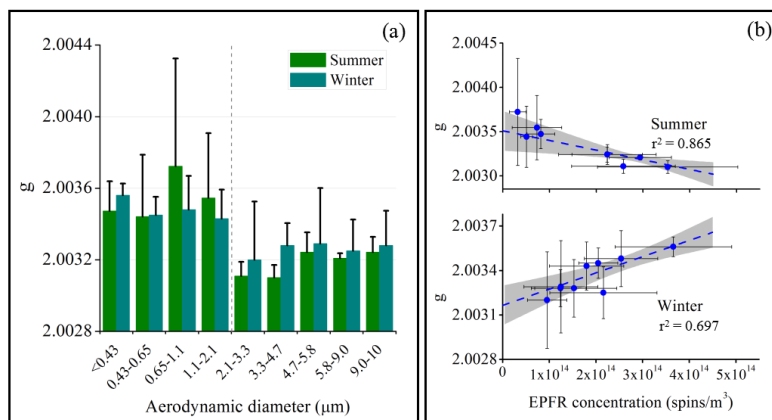


- 594 Tong, H., Lakey, P. S. J., Arangio, A. M., Socorro, J., Shen, F., Lucas, K., Brune, W. H., Pöschl, U.,  
595 Shiraiwa, M., 2018. Reactive oxygen species formed by secondary organic aerosols in water  
596 and surrogate lung fluid. *Environ. Sci. Technol.* 52 (20), 11642–11651.
- 597 Trapp, J. M., Millero, F. J., Prospero, J. M., 2010. Temporal variability of the elemental  
598 composition of African dust measured in trade wind aerosols at Barbados and Miami. *Mar.*  
599 *Chem.* 120 (1-4), 71–82.
- 600 Truong, H., Lomnicki, S., Dellinger, B., 2010. Potential for misidentification of environmentally  
601 persistent free radicals as molecular pollutants in particulate matter. *Environ. Sci. Technol.* 44  
602 (6), 1933–1939.
- 603 Valavanidis, A., Fiotakis, K., Vlachogianni, T., 2008. Airborne particulate matter and human health:  
604 toxicological assessment and importance of size and composition of particles for oxidative  
605 damage and carcinogenic mechanisms. *J. Environ. Sci. Heal. C.* 26 (4), 339–362.
- 606 Vejerano, E. P., Rao, G., Khachatryan, L., Cormier, S. A., Lomnicki, S., 2018. Environmentally  
607 persistent free radicals: Insights on a new class of pollutants. *Environ. Sci. Technol.* 52 (5),  
608 2468–2481.
- 609 Vejerano, E., Lomnicki, S. M., Dellinger, B., 2012a. Formation and stabilization of  
610 combustion-generated, environmentally persistent radicals on Ni(II)O supported on a silica  
611 surface. *Environ. Sci. Technol.* 46 (17), 9406–9411.
- 612 Vejerano, E., Lomnicki, S., Dellinger, B., 2011. Formation and stabilization of  
613 combustion-generated environmentally persistent free radicals on an Fe(III)2O3/silica surface.  
614 *Environ. Sci. Technol.* 45 (2), 589–594.
- 615 Valavanidis, A., Haralambous, E., 2001. A comparative study by electron paramagnetic resonance  
616 of free radical species in the mainstream and sidestream smoke of cigarettes with  
617 conventional acetate filters and 'bio-filters'. *Redox. Rep.* 6, 161–171.
- 618 Vejerano, E., Lomnicki, S., Dellinger, B., 2010. Formation and stabilization of  
619 combustion-generated environmentally persistent free radicals on an Fe(III) 2O3/silica  
620 surface. *Environ. Sci. Technol.* 45 (2), 589–594.
- 621 Vejerano, E., Lomnicki, S., Dellinger, B., 2012b. Lifetime of combustion-generated  
622 environmentally persistent free radicals on Zn(II)O and other transition metal oxides. *J.*  
623 *Environ. Monit.* 14 (10), 2803–2806.
- 624 Wang, P., Pan, B., Li, H., Huang, Y., Dong, X., Fang, A., Liu, L., Wu, Min., Xing, B., 2018. The  
625 overlooked occurrence of environmentally persistent free radicals in an area with low-rank  
626 coal burning, Xuanwei, China. *Environ. Sci. Technol.* 52 (3), 1054–1061.
- 627 Wang, Y., Li, S., Wang, M., Sun, H., Mu, Z., Zhang, L., Li, Y., Chen, Q., 2019. Source  
628 apportionment of environmentally persistent free radicals (EPFRs) in PM2.5 over Xi'an,  
629 China. *Sci. Total. Environ.* 689, 193–202.
- 630 Yang, L., Liu, G., Zheng, M., Jin, R., Zhu, Q., Zhao, Y., Wu, X., Yang, X., 2017. Highly elevated  
631 levels and particle-size distributions of environmentally persistent free radicals in  
632 haze-associated atmosphere. *Environ. Sci. Technol.* 51 (14), 7936–7944.
- 633 Yu, T., Wang, J., Shen, M., Li, W., 2013. NH3-SCR over Cu/SAPO-34 catalysts with various acid  
634 contents and low Cu loading. *Catal. Sci. Technol.* 3 (12), 3234–3241.



635

636 Figure 1. The concentration of EPFRs in PM with different particle sizes. (a) Atmospheric  
637 concentrations of EPFRs in different particle sizes in summer and winter. (b) The relative  
638 contribution of fine particles and coarse particles to the total EPFR concentration.



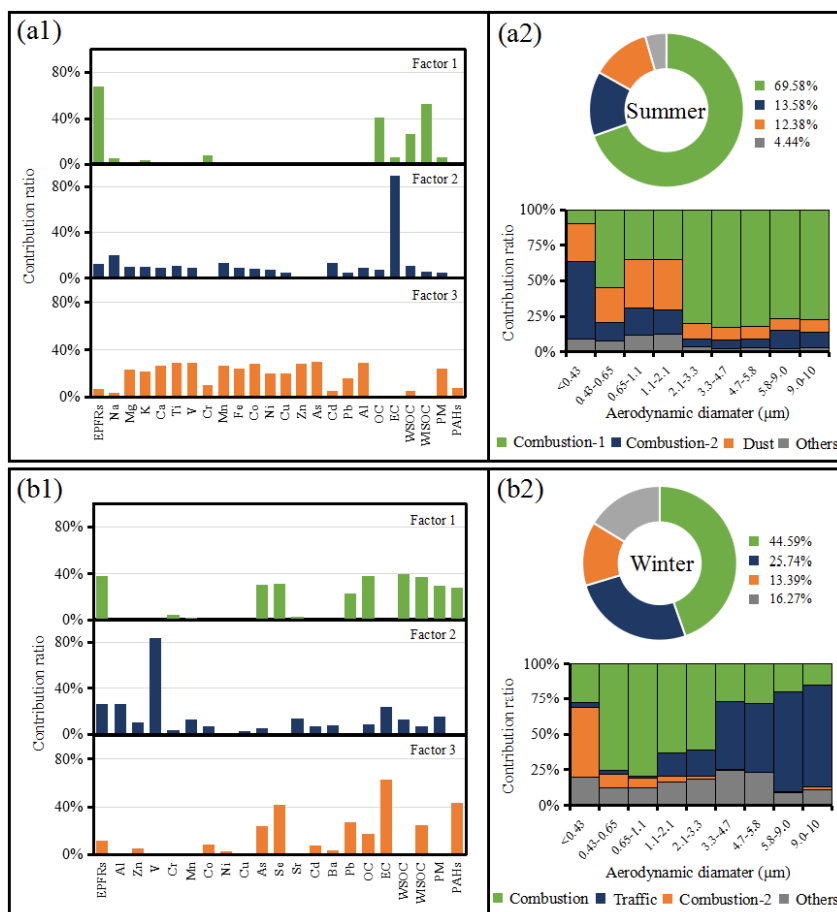
639

640 Figure 2. A  $g$ -factor comparison. (a) Comparison of  $g$ -factors of EPFRs in different particle sizes

641 in different seasons. (b) Correlation analysis of  $g$ -factors and concentrations of EPFRs in summer

642 and winter PM. The gray areas in the figure represent 95% confidence intervals.





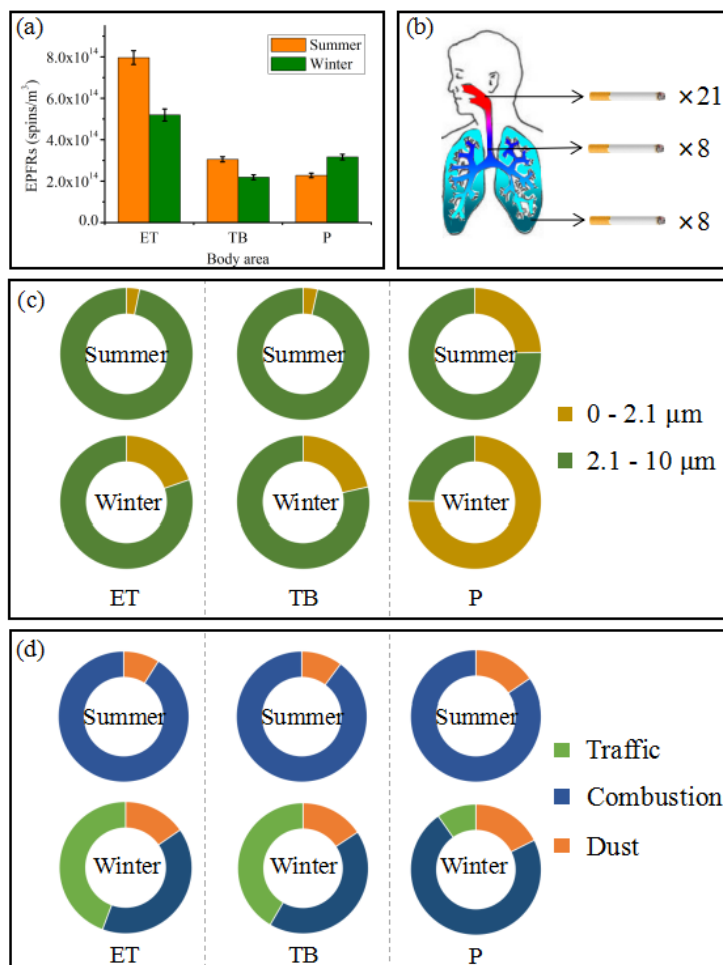
643

644 Figure 3. Factor analysis of EPFRs in different particle sizes in different seasons. (a1) and (b1)

645 represent the results of factor analysis for summer and winter, respectively. (a2) and (b2) represent

646 the contribution of various factors in summer and winter, respectively, to EPFRs and the relative

647 contributions of each factor for different particle sizes.



648  
 649 Figure 4. Exposure risks to EPFRs. (a) EPFR exposure in the ET, TB, and P regions. (b) Cigarette  
 650 exposure to EPFRs in the human respiratory system. (c) Exposure ratio of EPFRs with different  
 651 particle sizes in different areas of the respiratory system. (d) Contribution of EPFRs from different  
 652 sources to different areas of the respiratory system.